Control of mitochondrial metabolism and systemic energy homeostasis by microRNAs 378 and 378*

Michele Carrer[a], Ning Liu[a], Chad E. Grueter[a], Andrew H. Williams[a,1], Madlyn I. Frisard[b], Matthew W. Hulver[b], Rhonda Bassel-Duby[a], and Eric N. Olson[a,2]

[a]Department of Molecular Biology, University of Texas Southwestern Medical Center, Dallas, TX 75390 and [b]Department of Human Nutrition, Foods, and Exercise, Virginia Tech University, Blacksburg, VA 24061

Edited[†] by Bruce M. Spiegelman, Dana-Farber Cancer Institute/Harvard Medical School, Boston, MA, and approved August 7, 2012 (received for review May 7, 2012)

Obesity and metabolic syndrome are associated with mitochondrial dysfunction and deranged regulation of metabolic genes. Peroxisome proliferator-activated receptor γ coactivator 1β (PGC-1β) is a transcriptional coactivator that regulates metabolism and mitochondrial biogenesis through stimulation of nuclear hormone receptors and other transcription factors. We report that the *PGC-1β* gene encodes two microRNAs (miRNAs), miR-378 and miR-378*, which counterbalance the metabolic actions of PGC-1β. Mice genetically lacking miR-378 and miR-378* are resistant to high-fat diet-induced obesity and exhibit enhanced mitochondrial fatty acid metabolism and elevated oxidative capacity of insulin-target tissues. Among the many targets of these miRNAs, carnitine *O*-acetyltransferase, a mitochondrial enzyme involved in fatty acid metabolism, and MED13, a component of the Mediator complex that controls nuclear hormone receptor activity, are repressed by miR-378 and miR-378*, respectively, and are elevated in the livers of miR-378/378* KO mice. Consistent with these targets as contributors to the metabolic actions of miR-378 and miR-378*, previous studies have implicated carnitine *O*-acetyltransferase and MED13 in metabolic syndrome and obesity. Our findings identify miR-378 and miR-378* as integral components of a regulatory circuit that functions under conditions of metabolic stress to control systemic energy homeostasis and the overall oxidative capacity of insulin target tissues. Thus, these miRNAs provide potential targets for pharmacologic intervention in obesity and metabolic syndrome.

fatty acid oxidation | adipocytes | mitochondrial CO_2 production

Metabolic syndrome is a systemic disorder that includes a spectrum of abnormalities associated with obesity and type II diabetes. Defects in mitochondrial oxidative metabolism of fatty acids have been linked to diet-induced obesity and the development of insulin resistance in adipose tissue and skeletal muscle (1, 2). Consistent with the observation that mitochondrial dysfunction is a risk factor for the development of metabolic syndrome, obese individuals have mitochondria with compromised bioenergetic capacity (3–6).

Mitochondrial biogenesis, thermogenesis, and glucose and fatty acid metabolism are regulated by peroxisome proliferator-activated receptor γ coactivator 1 (PGC-1), a transcriptional coactivator that interacts with a broad range of transcription factors (7, 8). The PGC-1 family member PGC-1β is encoded by the *Ppargc1b* gene and is preferentially expressed in tissues with relatively high mitochondrial content, including heart, slow skeletal muscle, and brown adipose tissue (BAT) (9). Embedded in the first intron of the *Ppargc1b* gene are two microRNAs (miRNAs), miR-378 and miR-378*, which originate from a common hairpin RNA precursor (10). MiRNAs are ∼22-nt single-stranded RNAs that mediate the degradation or inhibition of specific target mRNAs (11–13). Approximately one-third of miRNAs are encoded by introns of protein-coding genes, and frequently intronic miRNAs have been found to modulate, either positively or negatively, the same biological processes as the protein encoded by the host gene (14–18).

Several miRNAs have been implicated in metabolic homeostasis based on loss-of-function studies in mice (16, 19, 20). MiR-33, encoded by an intron of the sterol regulatory element binding protein gene, has been shown to collaborate with sterol regulatory element binding protein to regulate intracellular cholesterol levels and lipid homeostasis by targeting the adenosine triphosphate-binding cassette transporter A1, a regulator of cellular cholesterol efflux (15). Other miRNAs have been linked to the regulation of glucose metabolism. Silencing of miR-103/107 improves glucose homeostasis and insulin sensitivity in mice (21). Lin28a, which inhibits processing of let-7 miRNA, promotes insulin signaling and confers resistance to high-fat diet (HFD)-induced diabetes (22). Conversely, let-7 overexpression impairs glucose tolerance and reduces insulin secretion in mice (22, 23). We recently reported that pharmacologic inhibition of miR-208a in mice confers resistance to obesity and improves insulin sensitivity (24). The influence of miR-208a on systemic energy homeostasis appears to be mediated, at least in part, by repression of MED13, a component of the Mediator complex that regulates nuclear receptor signaling (24, 25).

In the present study, we investigated the functions of miR-378 and miR-378* in mice by deleting these miRNAs, leaving the host gene *Ppargc1b* intact. We found that mice lacking miR-378 and miR-378* are protected against diet-induced obesity. Previous studies have identified numerous metabolic regulatory proteins as targets for repression by miR-378 and miR-378* (10, 26–28). In addition, we found that carnitine *O*-acetyltransferase (CRAT), a mitochondrial enzyme involved in fatty acid metabolism (29, 30), and MED13 are repressed by miR-378 and miR-378*, respectively. Our findings indicate that miR-378 and miR-378* function to control the overall oxidative capacity of metabolically active tissues during periods of dietary stress. These miRNAs thus serve as potential targets for pharmacologic intervention in obesity and metabolic syndrome.

Results

miR-378 and miR-378* Are Coregulated and Coexpressed with PGC-1β. miR-378 and miR-378* are generated from a common hairpin precursor RNA encoded by the first intron of the *Ppargc1b* (*PGC-1β*) gene and are coexpressed with PGC-1β (Fig. 1 *A* and *B*) (10). Although the miRNA* strand of most miRNA precursors is rapidly degraded, we were able to detect both miR-

Author contributions: M.C., N.L., C.E.G., A.H.W., R.B.-D., and E.N.O. designed research; M.C., N.L., C.E.G., and A.H.W. performed research; M.I.F. and M.W.H. contributed new reagents/analytic tools; M.C., N.L., R.B.-D., and E.N.O. analyzed data; and M.C., R.B.-D., and E.N.O. wrote the paper.

Conflict of interest statement: E.N.O. is a cofounder of miRagen Therapeutics, a company focused on developing miRNA-based therapies for cardiovascular disease.

[†]This Direct Submission article had a prearranged editor.

[1]Present address: Department of Biochemistry and Molecular Biophysics, Columbia University Medical Center, New York, NY 10032.

[2]To whom correspondence should be addressed. E-mail: Eric.Olson@utsouthwestern.edu.

This article contains supporting information online at www.pnas.org/lookup/suppl/doi:10.1073/pnas.1207605109/-/DCSupplemental.

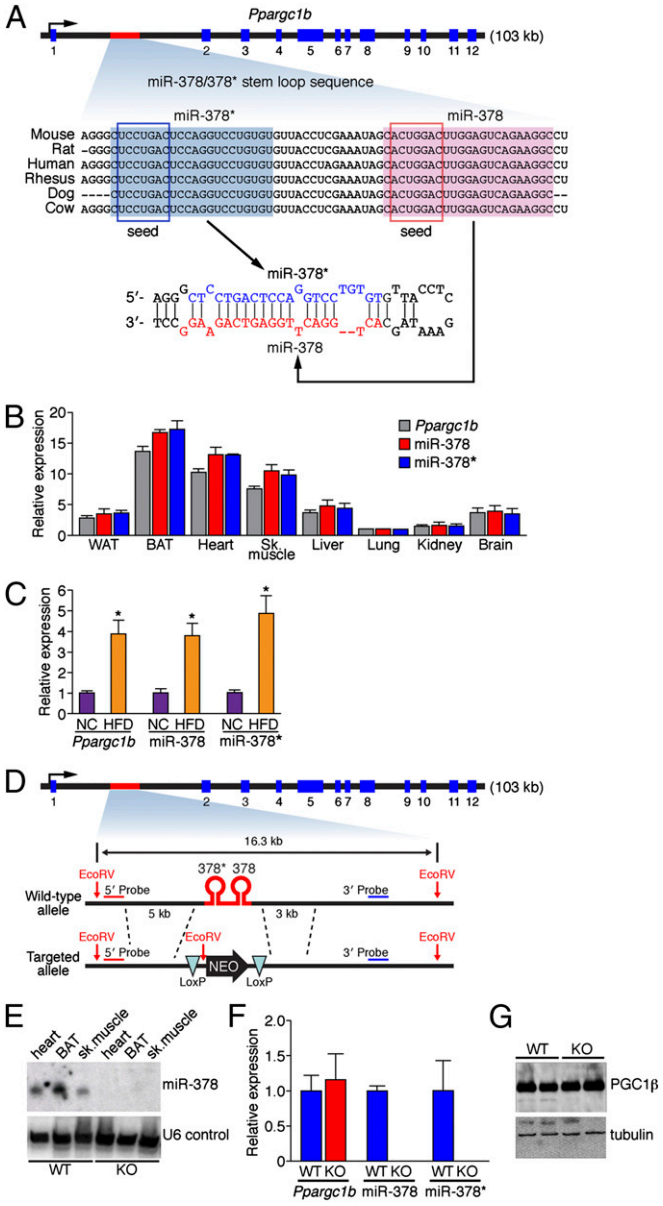

Fig. 1. Expression and genetic deletion of miR-378 and 378*. (*A*) The genomic locus encoding *Ppargc1b*, miR-378, and miR-378*. (*B*) Tissue distribution of *Ppargc1b*, miR-378, and miR-378*, detected by quantitative RT-PCR. (*C*) Up-regulation of miR-378, miR-378*, and *Ppargc1b* in the murine liver in response to HFD, detected by quantitative RT-PCR. (*D*) Targeting strategy used to generate miR-378/378* KO mice. The sequence of the entire hairpin structure encoding both miR-378 and miR-378* was replaced by a NEO cassette flanked by loxP sites via homologous recombination. The NEO cassette was subsequently removed using CAG-Cre recombinase. (*E*) Northern blot analysis of miR-378 in different tissues from WT and KO mice. U6 RNA was detected as a control. (*F*) Expression of *Ppargc1b*, miR-378, and miR-378* by quantitative RT-PCR in miR-378/378* WT and KO mice. (*G*) Western blot of heart isolated from miR-378/378* KO and WT mice using antibody against PGC-1β. Tubulin was used as a loading control. *$P < 0.05$.

378* and miR-378 in various tissues using quantitative RT-PCR (Fig. 1*B*). In response to HFD, *Ppargc1b*, miR-378, and miR-378* were up-regulated in parallel in the liver, consistent with the coregulation of these miRNAs and their host gene (Fig. 1*C*). In contrast, we did not detect regulation of these miRNAs in BAT, white adipose tissue (WAT), skeletal muscle, or heart in response to HFD (Fig. S1).

Genetic Deletion of miR-378/378* Confers Resistance to HFD-Induced Obesity. Given the importance of PGC-1β in the regulation of mitochondrial biogenesis and metabolism (31–33) and the importance of miRNAs in disease, we investigated the role of miR-378 and miR-378* under conditions of metabolic stress. To explore the functions of miR-378/378* in vivo, we used homologous recombination to delete the region of intron 1 of the *Ppargc1b* gene encoding miR-378/378* (Fig. 1*D*). Deletion of miR-378/378* was confirmed by Northern blot analysis and quantitative RT-PCR (Fig. 1 *E* and *F*). The targeted mutation did not alter the expression of PGC-1β mRNA or protein in tissues from homozygous mutant mice (Fig. 1 *F* and *G*). MiR-378/378* KO mice were born at normal Mendelian ratios and exhibited no overt abnormalities under basal conditions.

The functions of miRNAs may be accentuated under conditions of stress (34, 35). Consequently, we subjected miR-378/378* KO mice to metabolic stress by feeding an HFD. Whereas WT and mutant mice had comparable weights on normal chow, KO mice were resistant to obesity induced by the HFD (Fig. 2*A*). Body composition analysis by MRI revealed that the weight difference between miR-378/378* KO and WT mice after 8 wk on HFD was due to reduced mass of fat depots, with comparable

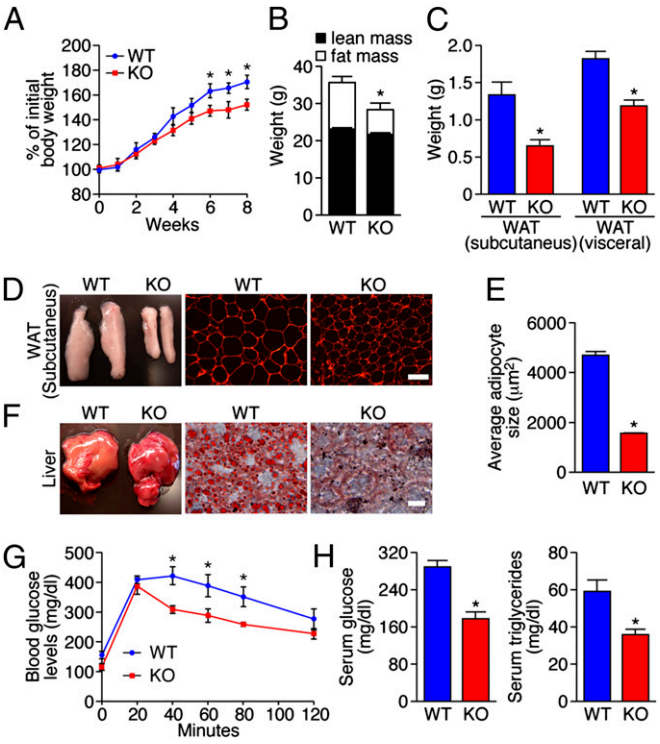

Fig. 2. MiR-378/378* KO mice are resistant to HFD-induced obesity and exhibit reduced obesity-associated insulin resistance. (*A*) MiR-378/378* KO mice gain less weight compared with WT mice on HFD. (*B*) MRI analysis of body composition in miR-378/378* KO and WT mice after 8 wk of HFD. (*C*) Weight of subcutaneous and visceral fat pads isolated from miR-378/378* KO and WT mice after 8 wk of HFD. (*D*) (*Left*) Subcutaneous fat pads from KO and WT mice. (*Middle* and *Right*) H&E-stained histological sections of visceral fat pads from miR-378/378* KO and WT mice after 8 wk of HFD. Pictures were taken using the rhodamine channel on a Leica DMRXE fluorescent microscope. (Scale bars: 100 μm.) (*E*) Difference in adipocyte size between WT and KO mice. (*F*) (*Left*) Liver from miR-378/378* KO and WT mice after 8 wk of HFD. (*Middle* and *Right*) Oil red O staining of histological liver sections from WT and KO mice after 8 wk of HFD. (Scale bar: 20 μm.) (*G*) Blood glucose levels in miR-378/378* KO and WT mice during a glucose tolerance test after 8 wk of HFD. (*H*) Random measurements of serum glucose and triglyceride levels in miR-378/378* KO and WT mice after 8 wk of HFD. *$P < 0.05$.

lean mass in the two groups (Fig. 2*B*). Both the subcutaneous and visceral WAT pads were smaller in the miR-378/378* KO mice on HFD compared with their WT littermates (Fig. 2 *C* and *D*). Histological analysis showed smaller white adipocytes in miR-378/378* KO mice on HFD compared with WT mice (Fig. 2 *D* and *E*). Gross anatomy of WT and KO mouse livers demonstrated reduced hepatic steatosis in the mutant mice after 8 wk of HFD (Fig. 2*F*). Oil red O staining of histological sections provided further evidence of reduced liver fat deposition in mutant mice compared with WT mice (Fig. 2*F*). H&E staining of histological sections of heart and skeletal muscle from WT and KO mice on HFD revealed no abnormalities in myofiber structure or organization (Fig. S2*A*). Oil red O staining of histological sections demonstrated no difference in ectopic lipid deposition in heart and skeletal muscle between WT mice and KO mice on HFD (Fig. S2*A*). Furthermore, no differences in lipid accumulation were detected between WT and KO after 8 wk of HFD, based on analysis of triglyceride content in cardiac tissue and quantitative RT-PCR for markers of fully differentiated lipid-storing cells, such as *aP2* and *Pparγ* (Fig. S2 *B* and *C*). Histological sections and quantitative RT-PCR for markers of inflammation also revealed no signs of inflammatory response in heart, skeletal muscle, liver, or WAT of WT or miR-378/378* KO mice after 8 wk of HFD (Fig. S2 *A* and *D*).

In humans and rodents, obesity is associated with reduced insulin sensitivity of target tissues. We tested whether genetic deletion of miR-378/378* in mice can improve the prediabetic state of insulin resistance associated with diet-induced obesity. We found that the absence of miR-378/378* increased the response to acute administration of glucose during glucose tolerance testing performed after 8 wk of HFD (Fig. 2*G*). In addition, glucose measurements after 8 wk of HFD confirmed reduced blood glucose levels in the miR-378/378* KO mice compared with WT controls (Fig. 2*H*). Serum triglycerides were also lower in miR-378/378* KO mice, suggesting global amelioration of the metabolic syndrome that accompanies obesity (Fig. 2*H*).

miR-378/378* KO Mice Display Increased Energy Expenditure and Mitochondrial Oxidative Capacity. To determine whether the obesity-resistant phenotype observed in miR-378/378* KO mice was related to enhanced activation of PGC-1β–controlled regulatory pathways in mitochondria, we measured whole-body energy consumption and mitochondrial number and function in mutant mice. Metabolic phenotyping revealed increased energy expenditure, as measured by body O_2 consumption and CO_2 production, in the mutant mice compared with WT controls on HFD (Fig. 3 *A* and *B*) with no difference in food intake (Fig. 3*C*). The overall increase in energy expenditure in KO mice compared with WT controls suggests that energy expenditure increases in response to the loss of miR-378/378* in one or more tissues in which PGC-1β is highly expressed (e.g., BAT, heart, skeletal muscle) or up-regulated (e.g., liver, WAT) on HFD and lipid accumulation (Fig. 1 *B* and *C* and Fig. S1*B*) (10, 26, 36).

The importance of PGC-1β in mitochondrial biogenesis is evident from the decreased mitochondria in liver, heart, and other tissues of mice with genetic deletion of PGC-1β (31–33). We found no difference in mitochondrial content of liver, heart, or skeletal muscle between miR-378/378* KO and WT mice, as measured by the ratio of mitochondrial DNA to genomic DNA (Fig. 3*D*). However, after isolation of mitochondria from liver of miR-378/378* KO and WT mice on HFD for 6 wk, we noted significantly greater mitochondrial function and oxidative capacity in the miR-378/378* KO mice (Fig. 3 *E*-*G*). Indeed, production of CO_2 and acid-soluble metabolites (ASMs) was higher in mitochondria isolated from the KO mice (Fig. 3 *E* and *F*). Similar results were obtained with whole-tissue lysates from slow skeletal muscle of the KO mice (Fig. 3 *E* and *F*). Taken together, these observations demonstrate an increase in the flux of metabolites through the mitochondria and an overall enhanced rate of complete fatty acid oxidation in the absence of miR-378/378*.

Our finding that production of ASMs was increased to a lesser extent than CO_2 production in the miR-378/378* KO mice suggests a parallel increase in the utilization of products of fatty acid β-oxidation through the tricarboxylic acid (TCA) cycle in these mice (37, 38). Therefore, we examined the expression of genes of the TCA cycle in hepatic tissue from mice lacking miR-378/378*. We found that two enzymatic components of the TCA cycle, *Sdhd* and *Fh1*, were up-regulated in the KO mice (Fig. 3*G*). We further examined the oxidative and glycolytic capacity of KO muscle fibers by quantitative RT-PCR for different myosin isoforms, as well as *Sox6* and *Slc2a4* (GLUT4), which are

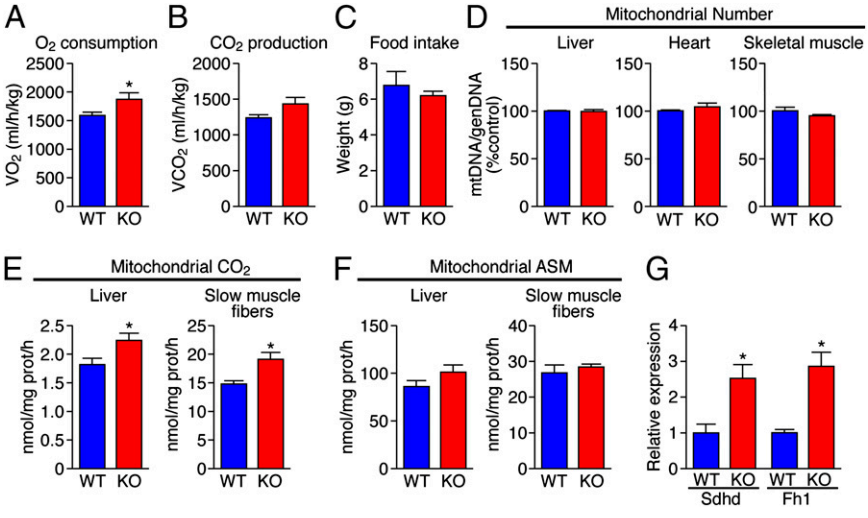

Fig. 3. Metabolic phenotyping and mitochondrial analysis in miR-378/378* KO mice. (*A*–*C*) Measurement of oxygen consumption (*A*), CO_2 production (*B*), and food intake (*C*) by metabolic chamber analysis of miR-378/378* KO and WT mice after 6 wk of HFD. (*D*) Assessment of mitochondrial number (expressed as the ratio of mitochondrial DNA to genomic DNA) in liver, heart, and skeletal muscle. (*E and F*) Measurement of CO_2 (*E*) and ASM production (*F*) in isolated mitochondria from the liver and in whole lysate from slow muscle fibers of miR-378/378* KO and WT mice after 6 wk of HFD. (*G*) Analysis of the expression of different genes of the TCA cycle in hepatic tissue from miR-378/378* KO compared with WT mice after 8 wk of HFD by quantitative RT-PCR. Sdhd, succinate dehydrogenase complex, subunit d; Fh1, fumarate hydratase 1. *$P < 0.05$.

involved in the specification of muscle fiber type and glucose uptake. We found no differences in the expression of these genes between the KO and WT mice on HFD (Fig. S3).

Crat and Med13 Are Among the Metabolic Targets of miR-378/378* miR-378 and miR-378* have different "seed" regions and thus target different mRNAs (Fig. 1*A*). Among the predicted targets of miR-378, the *Crat* mRNA contains a conserved miR-378 site in its 3′ UTR (Fig. 4*A*). CRAT channels the products of β-oxidation to the TCA cycle, away from mitochondrial efflux, thereby coupling mitochondrial fatty acid uptake to oxidative metabolism (29, 30, 39). Reduced CRAT activity has been identified as a reversible abnormality of the metabolic syndrome (29). Perturbation of metabolic homeostasis by HFD is associated with compromised mitochondrial fuel metabolism and incomplete fatty acid oxidation owing to reduced carnitine levels (29, 30). Up-regulation of *Crat* in the absence of miR-378 would be expected to contribute to the enhanced metabolic activity seen in these mutant mice (29).

We tested for repression of *Crat* by miR-378 by placing the 3′ UTR of the *Crat* mRNA downstream of a CMV-driven luciferase reporter. Luciferase assays revealed dose-dependent repression of the *Crat* 3′ UTR reporter by miR-378/378* (Fig. 4*B*). Mutation of the seed region in the *Crat* 3′ UTR reporter diminished the repression by miR-378/378* (Fig. 4*B*). Consistent with these findings, *Crat* mRNA was up-regulated in livers of mutant mice on HFD (Fig. 4*C*). Intriguingly, however, *Crat* expression was not significantly up-regulated in heart or skeletal muscle of miR-378/378* KO mice on HFD, further suggesting that miR-378 represses targets other than *Crat* in these tissues (Fig. S4*A*).

PGC-1β is an inducible coactivator of nuclear hormone receptors, which modulate metabolism via the Mediator complex (25, 40–43). MED13, a regulatory subunit of the Mediator complex, is a predicted target of miR-378*. MED13 has been linked to the maintenance of global energy homeostasis in *Drosophila* (44) and mice (24). The 3′ UTR of *Med13* mRNA contains three conserved sites recognized by the seed sequence of miR-378* (Fig. 4*D*). A luciferase reporter coupled to the 3′ UTR of the *Med13* gene was repressed on cotransfection of COS-1 cells with increasing amounts of pCMV-miR-378/378* (Fig. 4*E*). *Med13* mRNA expression was up-regulated in the hepatic tissue of miR-378/378* KO mice on HFD (Fig. 4*F*), consistent with a repressive influence of this miRNA on *Med13* in the liver. Similar to the findings for *Crat* expression, *Med13* was not significantly up-regulated in heart or skeletal muscle of miR-378/378* KO mice on HFD (Fig. S4*B*). We also found no increased expression of *Med13* or *Crat* in liver or other tissues from KO mice on normal chow. The absence of regulation of these miR-378/378* target genes under normal dietary conditions is consistent with the propensity of miRNAs to function selectively under stress (35). Consistently, we detected the most robust effect of miR-378/378* in liver, the organ in which these miRNAs are most up-regulated after HFD (Fig. 1*C*).

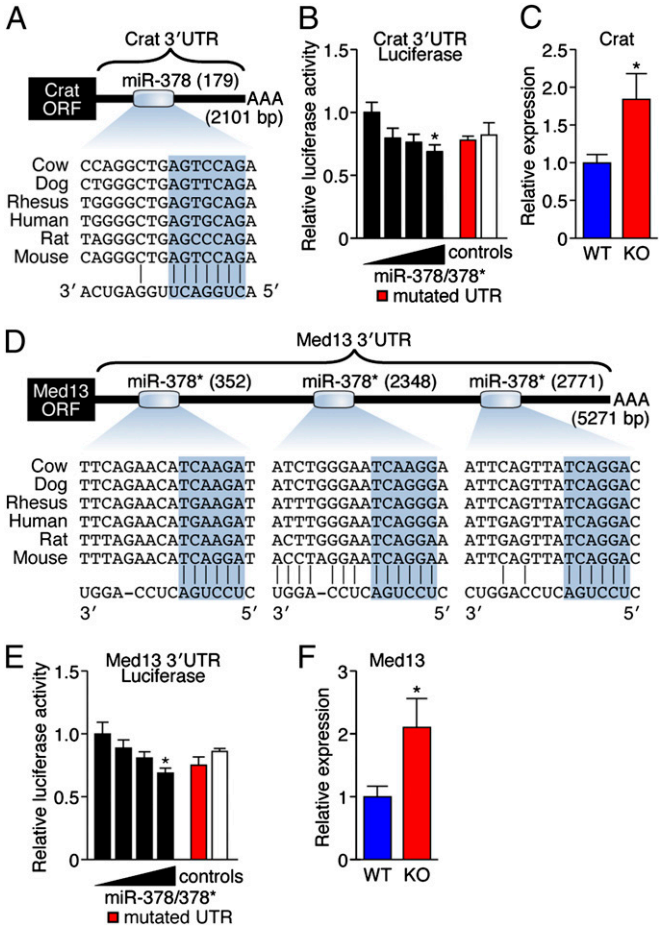

Fig. 4. Identification and validation of miR-378/378* targets. (*A*) Schematic diagram of the 3′ UTR of the *Crat* gene, highlighting the conserved miR-378 site. (*B*) Reporter assay measuring luciferase activity of the pMIR-reporter vector containing the *Crat* 3′ UTR in the presence of increasing amounts of pCMV-miR-378/378*. Mutations of the miR-378 site in the *Crat* 3′ UTR (red) and an unrelated miRNA (white) served as controls. (*C*) Quantitative RT-PCR of *Crat* expression in the liver of miR-378/378* KO compared with WT mice after 8 wk of HFD. (*D*) Schematic diagram of the 3′ UTR of the *Med13* gene, highlighting the three conserved miR-378* sites. (*E*) Luciferase activity of pMIR-reporter vector containing the *Med13* 3′UTR in the presence of increasing amounts of pCMV-miR-378/378*. Mutation of the miR-378* sites in the *Med13* 3′ UTR (red) and an unrelated miRNA (white) are controls. (*F*) Quantitative RT-PCR of *Med13* expression in the liver of miR-378/378* KO compared with WT mice after 8 wk of HFD. $*P < 0.05$.

Discussion

Our findings indicate that miR-378 and miR-378* participate in the regulation of mitochondrial metabolism and energy homeostasis in mice through the transcriptional network controlled by PGC-1β (Fig. 5). MiR-378/378* KO mice are protected against HFD-induced obesity and exhibit enhanced mitochondrial fatty acid metabolism in liver and slow muscle fibers.

Like other miRNAs, miR-378 and miR378* have numerous targets. Thus, although the repressive influence of these miRNAs on *Crat* and *Med13* in the liver likely contributes to their metabolic actions, the combined functions of these miRNAs in multiple tissues and on multiple targets are undoubtedly involved as well. In this regard, we detected no changes in expression of *Crat* or *Med13* in muscle tissues of miR-378/378* mutant mice. Given the sensitivity of miRNA-dependent repression to stress signaling (35), the apparent restriction of *Crat* and *Med13* regulation to the liver may indicate greater sensitivity of this tissue to the adverse consequences of an HFD. In agreement with our findings, miR-378* has been shown to target the mRNAs encoding estrogen-related receptor-γ and GA-binding protein-α, which associate with PGC-1β to control oxidative metabolism (10). Up-regulation of miR-378* in cancer cells has been proposed to mediate increased lactate production owing to the shift from oxidative to glycolytic metabolism, known as the Warburg effect, which is associated with tumorigenesis (10, 45). Thus, the phenotype resulting from increased miR-378* expression is the reciprocal to the shift toward oxidative metabolism that we observed on genetic deletion of miR-378*. In addition, miR-378 targets the transcriptional repressor MyoR during myoblast differentiation, increasing the activity of the myogenic transcription factor MyoD, which in turn up-regulates miR-378 within a regulatory feed-forward loop (46). Furthermore, miR-378 has been reported

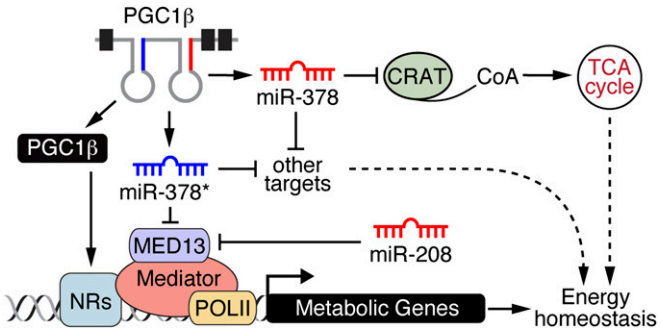

Fig. 5. Schematic diagram of the roles of miR-378 and miR-378* in energy homeostasis and mitochondrial functions. PGC-1β is a transcriptional coactivator of nuclear hormone receptors (NRs), which modulate metabolism via the Mediator complex and the basal transcription machinery. MED13, a subunit of the Mediator complex, is a target of miR-378*, and *Crat* is a target of miR-378. CRAT is a mitochondrial enzyme involved in fatty acid oxidative metabolism via the TCA cycle. Thus, miR-378 and miR-378* are integral components of a regulatory circuit that functions under conditions of metabolic stress to control the overall oxidative capacity of insulin target tissues.

to target the insulin-like growth factor 1 receptor and to promote apoptosis in cardiomyocytes (28).

Our global genetic deletion of the miR-378/378* cluster leaves open questions regarding the relative contributions of miR-378 and miR-378* in different insulin target tissues. For example, these miRNAs might have unrecognized functions in the brain that influence energy homeostasis. In addition, we noted a reduction of adipocyte size in mice lacking miR-378/378*, raising the possibility that these miRNAs are required for efficient hypertrophy and lipid uptake in white adipocytes. In this regard, overexpression of miR-378/378* in mesenchymal precursor cells has been shown to increase lipogenesis (26). The modulation of fatty acid metabolism by miR-378/378* is crucial not only in the context of adipogenesis, but also in the maintenance of cardiac function, given that the adult heart depends primarily on fatty acids as an energy source (47). Thus, it will be of eventual interest to investigate the potential influence of these miRNAs on cardiac function and pathological remodeling under conditions of nutritional and other forms of stress.

We recently reported that MED13 is also a target of miR-208a and other muscle-specific miRNAs encoded by introns of myosin heavy-chain genes (24). Up-regulation of MED13 in the heart through transgenic overexpression or miR-208a inhibition was found to confer resistance to HFD. Thus, MED13 serves as a nodal point for the convergence of multiple miRNAs to modulate energy balance and metabolism.

MiR-378/378* mutant mice, like other mouse strains lacking specific miRNAs (35), do not display overt phenotypes under normal laboratory conditions, but phenotypes become apparent under conditions of stress—in this case, in response to excessive calorie intake. Thus, miR-378 and 378* represent intriguing targets for disease modulation and pharmacologic intervention in the treatment of metabolic syndrome. However, the myriad targets of these miRNAs, as well as their expression in multiple tissues raises questions about systemic inhibition of these miRNAs with inhibitory oligonucleotides and their potential to modulate both pathological and beneficial processes in different tissues. Studies assessing the potential efficacy of systemically delivered miR-378/378* inhibitors in the setting of obesity, as well as their potential adverse side effects, are underway.

Methods

Generation of miR-378/378* KO Mice. The targeting vector used to generate the null allele of miR-378 and miR-378* was constructed using the pGKNEO-F2DTA plasmid, which contains a neomycin resistance gene driven by the pGK promoter, flanked by loxP sites, and a diphtheria toxin gene cassette. The miR-378/378* targeting strategy was designed to replace the premiR sequence with the neomycin resistance cassette flanked by loxP sites. The 5′ and 3′ arms of homology were generated by Taq LA PCR amplification (TaKaRa) using 129SvEv genomic DNA. The targeting vectors were electroporated into 129SvEv-derived ES cells. Five-hundred ES cell clones were analyzed for homologous recombination by Southern blot analysis. Three clones with the targeted miR-378/378* allele were injected into 3.5-d-old C57BL/6 blastocysts by the Transgenic Technology Center at University of Texas Southwestern Medical Center. High-percentage chimeric male mice were crossed to C57BL/6 females to achieve germline transmission of the targeted allele. Heterozygous neo$^+$ mice were intercrossed with CAG-Cre-transgenic mice to remove the neo cassette. Studies were performed with mice in 129SvEv/C57BL/6 mixed backgrounds. All experimental procedures involving animals in this study were reviewed and approved by the University of Texas Southwestern Medical Center's Institutional Animal Care and Research Advisory Committee.

HFD, Glucose Tolerance Test, and Glucose and Triglyceride Measurements. Mice were fed a rodent diet containing 45% kcal from fat (Open Source Diets) for the specified time. Glucose tolerance tests were performed by i.p. injection of glucose (1.5 g/kg) following an overnight fast. Serum triglycerides levels were measured using the Ortho Vitros 250 chemistry system. To measure triglycerides in the heart, tissue specimens were frozen immediately after isolation. Serum and tissue triglyceride levels were measured at the Mouse Metabolic Phenotyping Core at University of Texas Southwestern Medical Center.

Histological Analysis. Subcutaneus fat pads were harvested, fixed in 4% (vol/vol) paraformaldehyde for 24 h, and processed for routine paraffin histology. Sections were stained with H&E following standard procedures. For neutral lipid staining, liver was harvested and flash-frozen in embedding medium containing a 3:1 mixture of Tissue Freezing Medium (Triangle Biomedical Sciences) and gum tragacanth (Sigma-Aldrich). Frozen sections were cut on a cryotome and stained with oil red O. For adipocyte size analysis, the cell area was measured using ImageJ software from pictures of H&E sections obtained with a Leica DMRXE fluorescence microscope using the rhodamine channel.

Metabolic Chambers and Whole-Body Composition Analysis. Metabolic phenotyping of WT and miR-378/378* KO mice on HFD was performed using TSE metabolic chamber analysis at the Mouse Metabolic Phenotyping Core at University of Texas Southwestern Medical Center. Whole-body composition parameters were measured by MRI using a Bruker Minispec mq10 system.

Mitochondria Isolation from Liver. Mitochondria were isolated from liver of 10-wk-old WT and miR-378/378* KO mice as described previously (48), with modifications. Tissue samples were collected in buffer containing 67 mM sucrose, 50 mM Tris/HCl, 50 mM KCl, 10 mM EDTA/Tris, and 10% (wt/vol) BSA. Samples were minced and digested in 0.05% trypsin for 30 min, then homogenized. Mitochondria were isolated by differential centrifugation, and mitochondrial content was measured by quantitative RT-PCR and expressed as a ratio of mitochondrial DNA to genomic DNA.

Fatty Acid Metabolism in Isolated Mitochondria. Fatty acid oxidation was assessed in isolated mitochondria by measuring and summing $^{14}CO_2$ production and ^{14}C-labeled ASMs from the oxidation of [1-^{14}C]-palmitic acid as described previously (49, 50).

Cell Culture, Transfection, and Luciferase Assay, DNA fragments containing full-length 3′ UTRs for putative miR-378 and miR-378* targets were cloned into the pMIR-REPORT vector (Ambion). Mutagenesis of the miR-378 or miR-378* binding sites, cell culture, and luciferase assays were performed as described previously (51). Whole-cell extracts were assayed for luciferase expression using a Promega Luciferase Assay Kit. Relative reporter activities are expressed as luminescence units normalized for β-gal expression.

Statistics. Data are presented as mean ± SEM. Differences between groups were tested for statistical significance using the unpaired two-tailed Student *t* test. P values < 0.05 were considered to indicate significance.

ACKNOWLEDGMENTS. We thank Steven Kliewer, Michael Haberland, Douglas Millay, Craig Malloy, Viviana Moresi, and James A. Richardson for insightful discussions; Ryan McMillan, Cheryl Nolen and John McAnally for technical support; and Jose Cabrera for graphics. M.C. was supported by a Predoctoral Fellowship from the American Heart Association. Work in the laboratory of Eric Olson was supported by grants from the National Institutes of Health, Robert A. Welch Foundation (Grant I-0025), American

Heart Association, Jon Holden DeHaan Foundation, Donald W. Reynolds Center for Clinical Cardiovascular Research, Fondation Leducq TransAtlantic Network of Excellence in Cardiovascular Research Program, and Cancer Prevention and Research Institute of Texas.

1. Kusunoki J, Kanatani A, Moller DE (2006) Modulation of fatty acid metabolism as a potential approach to the treatment of obesity and the metabolic syndrome. *Endocrine* 29:91–100.
2. Maassen JA, Romijn JA, Heine RJ (2007) Fatty acid-induced mitochondrial uncoupling in adipocytes as a key protective factor against insulin resistance and beta cell dysfunction: A new concept in the pathogenesis of obesity-associated type 2 diabetes mellitus. *Diabetologia* 50:2036–2041.
3. Anderson EJ, et al. (2009) Mitochondrial H_2O_2 emission and cellular redox state link excess fat intake to insulin resistance in both rodents and humans. *J Clin Invest* 119: 573–581.
4. Bonnard C, et al. (2008) Mitochondrial dysfunction results from oxidative stress in the skeletal muscle of diet-induced insulin-resistant mice. *J Clin Invest* 118:789–800.
5. Gianotti TF, et al. (2008) A decreased mitochondrial DNA content is related to insulin resistance in adolescents. *Obesity (Silver Spring)* 16:1591–1595.
6. Li J, et al. (2010) Cardiolipin remodeling by ALCAT1 links oxidative stress and mitochondrial dysfunction to obesity. *Cell Metab* 12:154–165.
7. Finck BN, Kelly DP (2006) PGC-1 coactivators: Inducible regulators of energy metabolism in health and disease. *J Clin Invest* 116:615–622.
8. Handschin C, Spiegelman BM (2006) Peroxisome proliferator-activated receptor gamma coactivator 1 coactivators, energy homeostasis, and metabolism. *Endocr Rev* 27:728–735.
9. Esterbauer H, Oberkofler H, Krempler F, Patsch W (1999) Human peroxisome proliferator activated receptor gamma coactivator 1 (PPARGC1) gene: cDNA sequence, genomic organization, chromosomal localization, and tissue expression. *Genomics* 62: 98–102.
10. Eichner LJ, et al. (2010) miR-378(*) mediates metabolic shift in breast cancer cells via the PGC-1β/ERRγ transcriptional pathway. *Cell Metab* 12:352–361.
11. Bartel DP (2004) MicroRNAs: Genomics, biogenesis, mechanism, and function. *Cell* 116:281–297.
12. Djuranovic S, Nahvi A, Green R (2011) A parsimonious model for gene regulation by miRNAs. *Science* 331:550–553.
13. Filipowicz W, Bhattacharyya SN, Sonenberg N (2008) Mechanisms of post-transcriptional regulation by microRNAs: Are the answers in sight? *Nat Rev Genet* 9:102–114.
14. Dill H, Linder B, Fehr A, Fischer U (2012) Intronic miR-26b controls neuronal differentiation by repressing its host transcript, ctdsp2. *Genes Dev* 26:25–30.
15. Najafi-Shoushtari SH, et al. (2010) MicroRNA-33 and the SREBP host genes cooperate to control cholesterol homeostasis. *Science* 328:1566–1569.
16. Small EM, Olson EN (2011) Pervasive roles of microRNAs in cardiovascular biology. *Nature* 469:336–342.
17. van Rooij E, et al. (2009) A family of microRNAs encoded by myosin genes governs myosin expression and muscle performance. *Dev Cell* 17:662–673.
18. Wang S, et al. (2008) The endothelial-specific microRNA miR-126 governs vascular integrity and angiogenesis. *Dev Cell* 15:261–271.
19. Näär AM (2011) MiRs with a sweet tooth. *Cell Metab* 14:149–150.
20. Rottiers V, Näär AM (2012) MicroRNAs in metabolism and metabolic disorders. *Nat Rev Mol Cell Biol* 13:239–250.
21. Trajkovski M, et al. (2011) MicroRNAs 103 and 107 regulate insulin sensitivity. *Nature* 474:649–653.
22. Zhu H, et al.; DIAGRAM Consortium; MAGIC Investigators (2011) The Lin28/let-7 axis regulates glucose metabolism. *Cell* 147:81–94.
23. Frost RJ, Olson EN (2011) Control of glucose homeostasis and insulin sensitivity by the Let-7 family of microRNAs. *Proc Natl Acad Sci USA* 108:21075–21080.
24. Grueter CE, et al. (2012) A cardiac microRNA governs systemic energy homeostasis by regulation of MED13. *Cell* 149:671–683.
25. Ito M, Roeder RG (2001) The TRAP/SMCC/Mediator complex and thyroid hormone receptor function. *Trends Endocrinol Metab* 12:127–134.
26. Gerin I, et al. (2010) Roles for miRNA-378/378* in adipocyte gene expression and lipogenesis. *Am J Physiol Endocrinol Metab* 299:E198–E206.
27. John E, et al. (2012) Dataset integration identifies transcriptional regulation of microRNA genes by PPARγ in differentiating mouse 3T3-L1 adipocytes. *Nucleic Acids Res* 40:4446–4460.
28. Knezevic I, et al. (2012) A novel cardiomyocyte-enriched microRNA, miR-378, targets insulin-like growth factor 1 receptor: Implications in postnatal cardiac remodeling and cell survival. *J Biol Chem* 287:12913–12926.
29. Noland RC, et al. (2009) Carnitine insufficiency caused by aging and overnutrition compromises mitochondrial performance and metabolic control. *J Biol Chem* 284: 22840–22852.
30. O'Donnell JM, Alpert NM, White LT, Lewandowski ED (2002) Coupling of mitochondrial fatty acid uptake to oxidative flux in the intact heart. *Biophys J* 82:11–18.
31. Lelliott CJ, et al. (2006) Ablation of PGC-1beta results in defective mitochondrial activity, thermogenesis, hepatic function, and cardiac performance. *PLoS Biol* 4:e369.
32. Sonoda J, Mehl IR, Chong LW, Nofsinger RR, Evans RM (2007) PGC-1beta controls mitochondrial metabolism to modulate circadian activity, adaptive thermogenesis, and hepatic steatosis. *Proc Natl Acad Sci USA* 104:5223–5228.
33. Vianna CR, et al. (2006) Hypomorphic mutation of PGC-1beta causes mitochondrial dysfunction and liver insulin resistance. *Cell Metab* 4:453–464.
34. Leung AK, Sharp PA (2010) MicroRNA functions in stress responses. *Mol Cell* 40: 205–215.
35. Mendell JT, Olson EN (2012) MicroRNAs in stress signaling and human disease. *Cell* 148:1172–1187.
36. Haberland M, Carrer M, Mokalled MH, Montgomery RL, Olson EN (2010) Redundant control of adipogenesis by histone deacetylases 1 and 2. *J Biol Chem* 285:14663–14670.
37. Koves TR, et al. (2005) Peroxisome proliferator-activated receptor-gamma co-activator 1alpha-mediated metabolic remodeling of skeletal myocytes mimics exercise training and reverses lipid-induced mitochondrial inefficiency. *J Biol Chem* 280: 33588–33598.
38. Vergnes L, Chin R, Young SG, Reue K (2011) Heart-type fatty acid-binding protein is essential for efficient brown adipose tissue fatty acid oxidation and cold tolerance. *J Biol Chem* 286:380–390.
39. Cordente AG, et al. (2004) Redesign of carnitine acetyltransferase specificity by protein engineering. *J Biol Chem* 279:33899–33908.
40. Ge K, et al. (2002) Transcription coactivator TRAP220 is required for PPAR gamma 2-stimulated adipogenesis. *Nature* 417:563–567.
41. Malik S, et al. (2004) Structural and functional organization of TRAP220, the TRAP/mediator subunit that is targeted by nuclear receptors. *Mol Cell Biol* 24:8244–8254.
42. Malik S, Roeder RG (2010) The metazoan Mediator co-activator complex as an integrative hub for transcriptional regulation. *Nat Rev Genet* 11:761–772.
43. Wang Q, Sharma D, Ren Y, Fondell JD (2002) A coregulatory role for the TRAP-mediator complex in androgen receptor-mediated gene expression. *J Biol Chem* 277: 42852–42858.
44. Pospisilik JA, et al. (2010) Drosophila genome-wide obesity screen reveals hedgehog as a determinant of brown versus white adipose cell fate. *Cell* 140:148–160.
45. Dang CV (2012) Links between metabolism and cancer. *Genes Dev* 26:877–890.
46. Gagan J, Dey BK, Layer R, Yan Z, Dutta A (2011) MicroRNA-378 targets the myogenic repressor MyoR during myoblast differentiation. *J Biol Chem* 286:19431–19438.
47. Lopaschuk GD, Ussher JR, Folmes CD, Jaswal JS, Stanley WC (2010) Myocardial fatty acid metabolism in health and disease. *Physiol Rev* 90:207–258.
48. Frezza C, Cipolat S, Scorrano L (2007) Organelle isolation: Functional mitochondria from mouse liver, muscle and cultured fibroblasts. *Nat Protoc* 2:287–295.
49. Frisard MI, et al. (2010) Toll-like receptor 4 modulates skeletal muscle substrate metabolism. *Am J Physiol Endocrinol Metab* 298:E988–E998.
50. Hulver MW, et al. (2005) Elevated stearoyl-CoA desaturase-1 expression in skeletal muscle contributes to abnormal fatty acid partitioning in obese humans. *Cell Metab* 2:251–261.
51. van Rooij E, et al. (2008) Dysregulation of microRNAs after myocardial infarction reveals a role of miR-29 in cardiac fibrosis. *Proc Natl Acad Sci USA* 105:13027–13032.